# CHAPTER 4

# To study the *in silico* anti-inflammatory activity of the norabogori extract

## 4.1 Introduction:

Inflammation is an immunological defense mechanism against injury, burns, allergies, or microbial infections [1]. It is crucial to the pathophysiology of many illnesses, such as diabetes, cancer, and neurodegenerative cardiovascular disorders [2]. Acute inflammation occurs quickly and is crucial for wound healing, however chronic inflammation causes persistent discomfort that is typically associated with conditions including cancer, rheumatoid arthritis, osteoarthritis, and others [3]. The interaction of multiple processes during inflammation, including the activation of enzymes and release of different chemical mediators, cell migration, the release of fluids, and tissue injury and healing, is a complex phenomenon [4]. Inflammation is typically characterised by redness, swelling, discomfort, and fever. Several inflammatory mediators, including PGE2, tumor necrosis factor (TNF), interleukin-1 (IL-1), interleukin-6 (IL-6), and interleukin-10 (IL-10) activate macrophages, which are crucial in inflammation [5]. The enzyme prostaglandin synthase-2 (PTGS-2), also known as cyclooxygenase-2 (COX-2), is in charge of producing prostaglandins after inflammation. The rate-limiting phase in the generation of inflammatory prostaglandins is caused by the activation of PTGS-2, which is brought on by the activation of cytokines, mitogens, and endotoxins [6] Following the development of inflammation in inflammatory cells, its transcription may become active [7].

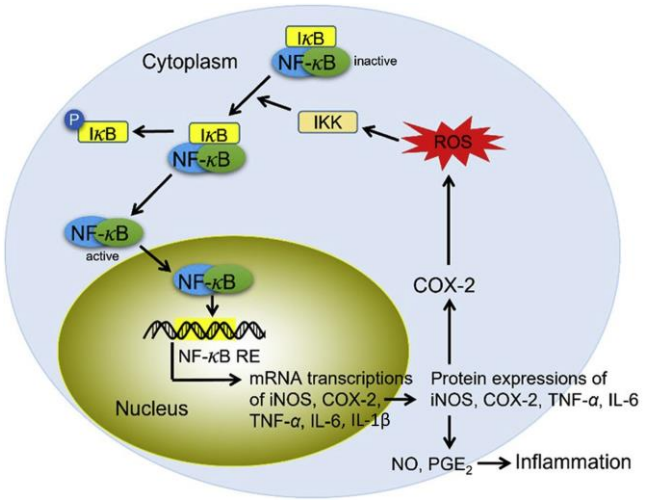


**Fig.4.1 Anti-inflammatory mechanism of the COX-2 inhibitor through cytokines [8]**

Anti-inflammatory medications, both steroidal and non-steroidal, have been used unsuccessfully to treat chronic inflammatory diseases such rheumatoid arthritis (RA) and atopic dermatitis (AD), as well as causing unforeseen side effects [9,10]. The treatment of these inflammatory illnesses is crucial. Chronic disorders like atherosclerosis, obesity, diabetes, neurological diseases, and occasionally cancer are all linked to inflammation [10].

Plants produce biologically active chemicals that are beneficial for human health and the treatment of a range of ailments in addition to producing essential nutrients for humans1. The medicinal plants include a wide variety of bioactive compounds that have the potential to be antibacterial, anticancer, anti-inflammatory, and antioxidant. Plants are a great source of beneficial bioactive compounds that can be used to make new chemotherapy medicines [11]. A crucial procedure is the examination of the potential use of pharmacologically potent substances obtained from medicinal plants [12]. Due to its high efficacy, low cost, non-narcotic origin, and little side effects, it is estimated that 80% of the world's population uses medicinal herbs [13]. The term "medicinal foods" refers to a variety of food crops that are utilised in medicine. Crude extracts from plants that contain a complex blend of different phytochemicals are widely used to make plant-derived medications, which are used to treat both chronic and infectious diseases. There is a huge variety of secondary metabolites present in different plant species, but only a small number of them have been investigated and shown to represent a significant source of bioactive molecules. When identifying different chemicals from plant extracts, such as alkaloids, flavonoids, organic acids, amino acids, etc., GC-MS is a trustworthy technique [14].

*In silico* predictions of pharmacological, pharmacokinetic, and toxicological properties are made using computational prediction models, and these models are vital in the decision-making process that results in advancements in both technology and medicine [15]. At least in the absence of genuine models, such as pure *in vitro* models, computational biology and bioinformatics research are beneficial to examine potential interactions of biomolecules with chemicals, such as herbal active components. A quick and inexpensive method for developing and testing medications is molecular docking. This method provides information on how drugs interact with receptors, which can be used to predict how a drug model will bind to a target protein [16], resulting in dependable binding at ligand binding sites. Finding anti-inflammatory elements that can be used to treat these disorders is urgently needed given the current circumstances [10]. Phenolic

compounds have been suggested as an alternative to prevent or treat chronic inflammatory diseases because, among many other biological/pharmacological properties, they are thought to have anti-inflammatory and immunomodulatory activity and have long been used in Chinese medicine [9,10]. These qualities have primarily been linked to flavonoids, and prior research has demonstrated their effectiveness in animal models. In certain experimental animal models, persistent inflammation has even been suppressed. For instance, kaempferol, rutin, and quercetin have all been investigated in cell cultures and animal models. Quercetin reduced edema in animal models of chronic conditions, including arthritis, and rutin was helpful in such conditions.

These health advantages are attributed to flavonols' anti-oxidant and radical-scavenging properties, regulation of inflammatory cell activity, NOS, modulation of arachidonic acid metabolism enzyme activity (phospholipase A2, cyclooxygenase, lipoxygenase), modulation of the production of pro-inflammatory molecules, and modulation of pro-inflammatory gene expression [9].

Reactive species are produced in response to tissue damage, which disrupts cellular processes and causes oxidative damage to nucleic acids, carbohydrates, and protein groups that are vulnerable to oxidation, such as the sulfhydryl group. ROS and NO anions are created by activated phagocytes and macrophages, respectively, during inflammation. Low-density lipoproteins (LDL) are immediately oxidized by NO, resulting in peroxynitrite, which permanently damages cell membranes. The ability of flavonoids to scavenge free radicals, including NO, and stop them from interacting with NO, limiting cell damage, can lessen this inflammatory effect. Furthermore, pro-inflammatory enzymes like phospholipase A2, cyclooxygenase, lipoxygenase, and iNOS can be modulated by flavonoids and other phenolic substances. It has been shown that certain flavonoids decrease the expression of genes that promote inflammation. Arachidonic acid, prostaglandins, leucotrienes, and NO important mediators of the inflammatory response are produced less when these enzymes are suppressed [9,10].

One crucial aspect of flavonoids' immune-modulating function is their capacity to inhibit these enzymes. The first flavonoid known to inhibit phospholipase A2 in human neutrophils was quercetin. Given that this enzyme is in charge of releasing arachidonic acid, the catalyst for inflammation, this ability is crucial. Prostaglandins, vasoactive leukotrienes, and thromboxanes are produced as a result of this acid's subsequent metabolism by cyclooxygenase isoforms and

lipoxygenase. Prostaglandins are significantly expressed in inflammation and are generated by the cyclooxygenase isoform cyclooxygenase-2.

In addition to quercetin, kaempferol, and rutin, the peach's peel and fresh pulp-derived compounds exhibited notable protection against oxidative damage to lipids and proteins when consumed on a regular basis. Additionally, it demonstrated significant anti-inflammatory activity by inhibiting inflammatory mediators including nuclear factor B (NF-B), interleukin-1 (IL-1), and tumour necrosis factor (TNF) [10,17,18]. FeSO4/H2O2 caused an inflammatory response in kidney, liver, and brain cortex tissues that resulted in a rise in TNF- and IL-1 levels. The release of these cytokines has been successfully stopped by peach suspensions [17].

Traditional methods for finding and screening phytochemicals for their medicinal effects were more expensive, time-consuming, and ineffective. More reasonable and successful approaches that rely on virtual screening have been devised to address the shortcomings of old approaches. Due to the availability of structural data on proteins and protein-ligand complexes through techniques of chemical synthesis, purification, X-ray crystallography, and Nuclear Magnetic Resonance Spectroscopy (NMR), a large variety of therapeutically significant molecular targets are known [19]. The interaction between the ligand and the target molecule is determined by the molecular docking technique. By identifying the preferred orientation of the minimal free binding energy, it predicts the binding affinity of the ligand to form a stable complex with the protein [20]. This interaction involves a variety of non-covalent interactions, including van der Waals, hydrophobic, ionic, and hydrogen bonds. Protein-protein, protein-ligand, and protein-nucleotide interactions are all candidates for molecular docking studies [21]. The molecular docking approach entails a number of processes, including the synthesis of ligands, determination of the binding energy of protein-ligand complexes, and result analysis [22].

Various programs such as DOCK [23], FLlexX [24], GOLD [25] and AutoDock [26] are used for successful docking studies. Prediction of the binding poses and affinities for effective binding into the target can reduce the efforts of experimental procedures for determination of accurate candidate with higher positive rates [27]. The optimization of its search method and its scoring function can help in determination of active bonded candidate for molecular docking studies [28-30]. The optimized algorithm helps in determination of its docking conformations with lower binding energies. Results are evaluated on the basis of its scoring function. In this study,

AutoDock 4.2 software was used to evaluate the molecular docking analysis. The hybrid algorithm of AutoDock 4.2 contains random drift particle swarm optimization and local search [31] and also Lamarckian genetic algorithm[26] as its search algorithm. Lamarckian genetic algorithm is an important energy search algorithm in AutoDock (Version 4.2) software. They mainly constitute of genetic algorithm along with the local search.

Molecular dynamics (MD) simulation is an important parameter for the study of the biological molecules that helps in calculation of the time dependent behavior of the molecules in a molecular environment. In this system, the atoms and its molecules move according to the influence of gravity which is run through a computer simulation program. The interaction of the motions of its atoms and molecules were visualized after being interacted for some time. The trajectories of the atoms and molecules were drawn using the Newton's numeric equations that are used for the system where the particles interact. For its calculations, the force field of the molecular mechanics in between the particles was used. This method is currently being used in physical chemistry, materials chemistry and biomolecules modeling although it was originally being used in the late 1950s in the field of theoretical physics [32]. This method was also used in the detailed study of the conformational changes of macromolecules [33]. These methods are now used for the investigation of the molecular dynamics and also the thermodynamics of the molecules and also their complexes. The study was used to understand the macromolecules that are obtained from X-ray crystallography and NMR experiments [34].

The objective of this study was to screen the Norabogori phytochemicals as potential inhibitor of anti-inflammatory target proteins like human Tumor necrosis factor α (TNF-α), Interleukin-1 β (IL1β) and Cyclooxygenase 2 (COX-2). Various properties such as Lipinski Rule of five, ADMET properties and docking study was carried out to screen molecules which could be used for development of TNFα,IL1β and COX-2 inhibitors. Molecular dynamics simulation was conducted to understand the behavior of the natural molecule inside the active site pocket of the protein. The interactions that are predicted through various docking procedures help in understanding the binding regions for increased accuracy of docking and hence could be used for cure of inflammatory diseases like inflammatory bowel disease.

## 4.2 MATERIALS AND METHODS

### 4.2.1 Phytochemical database preparation

The ligand database was prepared from earlier chromatography studies. We hypothesize that the naturally available molecules acting as natural inhibitors will be able to down regulate the expression of anti-inflammatory marker proteins targeted in the cell-line studies as explained in the previous chapter.

### 4.2.2 Evaluation of phytochemicals

In the evaluation of phytochemical compounds for their properties, first parameters were checking for the drug-likeness property. Using Lipinski's rule of five and Veber's rule, the compounds' drug-likeness was evaluated. This screening aids in the identification of substances that may exhibit low cellular absorption. The properties of Veber's rule and Lipinski's rule of five were computed using SwissADME, an open-source web resource [35]. The human body's Absorption, Distribution, Metabolism, and Excretion (ADME) system was used to anticipate how the ligands will behave there. ADME properties are important determinates for drug discovery and assessing the environmental hazards. Experimental validation of ADMET properties is costly and cannot meet the high demand for *in vitro* screening hence, computational methods can be an alternative to predict ADMET properties. In order to determine the ADMET properties, the SMILES format of the various compounds in the database was obtained from Pubchem (http://www.ncbi.nlm.nih.gov/pccompound) and deposited at the web server "admetSAR" (http://lmmd.ecust.edu.cn/admetsar2/) [36]. This helps in understanding if the compounds have any adverse side effect after its administration into the human body. For our work, we selected the following 9 parameters to screen the set of compounds: GI absorption, blood–brain barrier (BBB), P-glycoprotein substrate, Cytochrome inhibitors, and bioavailability score. The different toxicity profile of the compounds were also evaluated. The properties were ames mutagenesis, human intestinal absorption, acute oral toxicity, oral rat acute toxicity and hepatotoxicity. The phytochemicals were further treated as ligand for the docking studies.

### 4.2.3 Ligand structure retrieval:

The 3D structures of the compounds used for the virtual screening analysis were collected from PubChem (http://www.ncbi.nlm.nih.gov/pccompound) [37] in Structure Data File (SDF) format, which was later changed to Protein Data Bank (PDB) format by Open Babel software.

### 4.2.4 Ligand structure preparation:

Preparation of the ligand was carried out for the docking analysis. First step was the addition of hydrogen atoms and removal of water molecules. The non-polar hydrogens were merged and Gasteiger partial charges were added to it. Torsion forces were added to the ligands and the coordinates of the ligand were saved in PDBQT (Protein Data Bank, Partial Charge (Q), & Atom Type (T)) format. These structures were then used as the input structures during the docking study.

### 4.2.5 Protein structure retrieval

3D protein structures of *Homo sapiens* TNF-α, IL1β and COX-2 available on RCSB-Protein Data Bank (PDB) [https://www.rcsb.org/] were selected based on different features. First, the structures available were tabulated with their mutation, missing residue no. and resolution. The limiting factor which was first taken into action and strictly followed was mutation. Only the non-mutated structures were taken for consideration. When selecting the target PDB structure, the lowest resolution and lowest no. of missing residue no. were matched along with previous literature review.

### 4.2.6 Protein structure preparation

The crystallographic structures of the proteins were obtained from the database in Protein Data Bank (PDB) format [https://www.rcsb.org/]. Preparation of the protein was carried out for the docking experiments with the help of Chimera visualization software. The ligands attached to its active site residues were removed and the structure was saved in the PDBQT format.

### 4.2.7 Sequence alignment and homology modeling

The sequence of the target proteins were retrieved from UniProt. To identify the template, the obtained sequences were searched against Protein Data Bank (PDB) by BLASTP

(http://blast.ncbi.nlm.nih.gov/Blast.cgi. Homology Modeling 3D structure of target proteins have been predicted using Modeller9.10. Homology modeling of the proteins were performed by programs such as SWISS-MODEL [38] and MODELLER 9.10 [39]. Using MODELLER 9.10's linear gap penalty function, global dynamic programming was used to align the template and query sequences for model development [39]. The model's 'automodel' class was used to build it by satisfying spatial constraints. The script command in Python was utilized to create the model. To eliminate steric conflicts, the steepest descent energy minimization was used [40]. Finally the predicted models were evaluated based on their DOPE potential.

### 4.2.8 Molecular docking studies

Molecular docking studies were conducted to analyze protein–ligand complexes in the screening of ligands by an *in silico* approach. It is an important phenomenon for evaluation of molecules for determination of possible interactions with the active site residues of the protein molecule and shortlist them according to their highest binding affinities. Molecular docking was carried out by AutoDock Vina program and webserver Swissdock. Docking was done for all the 33 ligands by Autodock Vina first [38]. In order to obtain the right protein-ligand complex with the proper ligand orientation, AutoDock Vina use a Lamarckian genetic algorithm (LGA). The Broyden-Fletcher-Goldfarb-Shanno algorithm is used by AutoDock Vina. Both the protein and the ligands were initially energy reduced and then constructed with the aid of AutoDock. In the case of ligands, Gasteiger charges and nonpolar hydrogens were added, while water molecules were first removed from proteins before polar hydrogens and Kollman charges were added. During docking, default settings were applied. SwissDock is a web server which uses CHARMM (Chemistry at Harvard Macromolecular Mechanics) energy field on a specified grid for docking studies [41]. It is based on the EADock DSS engine, combined with setup scripts for curating common problems and for preparing both the target protein and the ligand input files. The ligands in docked complexes which showed lowest binding energy when evaluated by docking with Autodock Vina were taken up for further docking by SwissDock. Software like PyMol [38] and Discovery Studio Visualizer were then used to analyze the conformer with the lowest binding energy. The docked complex which was showing efficient binding with lowest energies simultaneously in both AutoDock and SwissDock were finally selected for molecular dynamic simulation studies.

### 4.2.9 Molecular dynamics simulation:

Molecular dynamics simulation is one of the most promising strategies for understanding the technical characteristics of the dynamics of molecules in biology. The analysis of the system's time-dependent state using MD simulation is possible. The dynamic behavior of biological macromolecules and ligands is examined in the MD modeling method in a time-dependent manner. By simulating atoms' actual state, the approach makes it easier to comprehend how they behave. Using a computational method, we may investigate how the protein interacts with its ligand throughout a given time period and gain knowledge about how stable the complexes are.

The protein structures that were modeled before docking with ligands and the docked complexes of proteins and ligands that were selected from the molecular docking scores stated earlier at 0, 50, and 100 ns are the structures that were simulated. The GROningen MAchine for Chemical Simulations (GROMACS) program (version 2020.435) was used to model the MD of all the atoms in the protein structure. We used the GROMOS 54a7 force field in the software packages GROMACS 2020.435 to run all-atom MD simulations to comprehend interactions between the ligand with target proteins. The force field parameters and topology of the ligand were built by the Automatic Topology Builder server (ATB, version 3.0) [40]. The generated topology file for the ligand contains details about partially charged atoms, dihedral, bond, and angle information. We chose the most stable complexes, namely, docked conformer with the minimum energy for MD simulations. The total charge is zero on the ligand. Simulation of ligand unbound target proteins in water were used as a control. Systems were kept 1 nm from the boundary of the box and solvated using the single point charge model (SPC). As conditions for periodic boundaries were maintained in overall directions, the LINCS technique was followed to limit all of the bonds [41]. Na+ ion was added as a counter ion before the simulation in the simulation box to balance the charges. Using a constraint of 1000 kJ $mol^{-1}$ $nm^{-1}$ in the steepest descent approach prior to equilibration the whole system's energy was minimized [42]. For temperature balancing aNVT run was done for 2 ns, and the pressure was adjusted using a 5 ns NPT run. Here we use the Parrinello–Rahman barostat algorithm [43], a velocity rescales thermostat [44] where the temperature is 300 K, and pressure were fixed to 1 bar, respectively. The equilibrium state complexes were used to perform 100 ns of MD simulation runs with a 2 femtosecond (fs) time step. The simulations were performed on a GPU-based system using a single NVIDIA Tesla K40

graphics card and 32 physical Intel-Xeon CPU cores. The final trajectories were evaluated using the GROMACS's tools, Grace and Chimera, along with Discovery Studio Visualizer (DSV) [37]. The visual representations were produced using PyMol software [Lyndem et al., 2023].

## 4.3 RESULTS AND DISCUSSION

### 4.3.1 Lipinski's Rule of Five and Veber's rule evaluation

In order to have drug likeness property and good ADMET properties, the log p values should be below 5, molecular weight should be below 500 kDa, hydrogen bond acceptor should be less than 10 whereas, hydrogen bond donor should be 5 whereas the Veber's rule parameters are rotatable bond count (≤10) and polar surface area (≤140 Å2). Out of the 33 molecules analysed from Norabogori it was found out that according to Lipinski rule of 5 and Veber's rule, though some compounds did not obey but the difference is negligible and taken up for further analysis.

**Table4.1 Lipinski rule of five evaluation of phytochemicals from norabogori extract**

| Name | MW | H-bond acceptors | H-bond donors | LogP |
|---|---|---|---|---|
| Oleanolic acid | 456.7 | 3 | 2 | 7.2336 |
| Ursolic acid | 456.7 | 3 | 2 | 7.0895 |
| Kojic acid | 142.11 | 4 | 2 | 6.206 |
| Maslinic acid | 472.7 | 4 | 3 | 6.2044 |
| α-Eleostearic acid | 278.43 | 2 | 1 | 5.6605 |
| (E)-parinaric acid | 276.41 | 2 | 1 | 5.4365 |
| Asiatic acid | 488.7 | 5 | 4 | 5.0327 |
| Propiomazine | 340.48 | 2 | 0 | 4.8321 |
| Kaempferol | 286.24 | 6 | 4 | 2.2824 |
| 4-trifluoromethylmandelic acid | 220.15 | 6 | 2 | 1.8234 |
| Coumarin | 146.14 | 2 | 0 | 1.793 |
| Ferulic acid | 194.18 | 4 | 2 | 1.4986 |
| 4-Hydroxycoumarin | 162.14 | 3 | 1 | 1.4986 |
| Ellagic acid | 302.19 | 8 | 4 | 1.3128 |
| Caffeic acid | 180.16 | 4 | 3 | 1.1956 |
| Syringic acid | 198.17 | 5 | 2 | 1.1076 |
| Nicotinic acid | 123.11 | 3 | 1 | 0.7798 |
| Gallic acid | 170.12 | 5 | 4 | 0.7637 |
| Adipic acid | 146.14 | 4 | 2 | 0.716 |
| Hederagenin | 472.7 | 4 | 3 | 0.5016 |

| | | | | |
|---|---|---|---|---|
| Arecoline | 155.19 | 3 | 0 | 0.4213 |
| Pipecolic acid | 129.16 | 3 | 2 | 0.2131 |
| Succinic acid | 118.09 | 4 | 2 | -0.0642 |
| L-Aspartic acid | 133.1 | 5 | 3 | -0.1623 |
| trans-Aconitic acid | 174.11 | 6 | 3 | -0.4433 |
| Chlorogenic acid | 354.31 | 9 | 6 | -0.6459 |
| citramalic acid | 148.11 | 5 | 3 | -0.7033 |
| (±)-Malic Acid | 134.09 | 5 | 3 | -1.0934 |
| D-(-)-Quinic acid | 192.17 | 6 | 5 | -1.127 |
| Citric acid | 192.12 | 7 | 4 | -1.2485 |
| Rutin | 610.52 | 16 | 10 | -1.6871 |
| Linamarin | 247.25 | 7 | 4 | -1.89492 |
| Furaneol | 128.13 | 3 | 1 | -2.3214 |
| Muramic acid | 251.23 | 8 | 5 | -2.7576 |

**Table4.2 Veber's Rule evaluation**

| Name | Rotatable bonds | TPSA (Å2 ) |
|---|---|---|
| 4-Hydroxycoumarin | 0 | 50.44 |
| Furaneol | 0 | 46.53 |
| Ellagic acid | 0 | 141.34 |
| Coumarin | 0 | 30.21 |
| D-(-)-Quinic acid | 1 | 118.22 |
| Gallic acid | 1 | 97.99 |
| Kojic acid | 1 | 70.67 |
| Maslinic acid | 1 | 77.76 |
| Nicotinic acid | 1 | 50.19 |
| Oleanolic acid | 1 | 57.53 |
| Pipecolic acid | 1 | 49.33 |
| Ursolic acid | 1 | 57.53 |
| Kaempferol | 1 | 111.13 |
| Arecoline | 2 | 29.54 |
| Asiatic acid | 2 | 97.99 |
| Caffeic acid | 2 | 77.76 |

| | | |
|---|---|---|
| Hederagenin | 2 | 77.76 |
| (±)-Malic Acid | 3 | 94.83 |
| 4-trifluoromethylmandelic acid | 3 | 57.53 |
| citramalic acid | 3 | 94.83 |
| L-Aspartic acid | 3 | 100.62 |
| Linamarin | 3 | 123.17 |
| Succinic acid | 3 | 74.6 |
| Syringic acid | 3 | 75.99 |
| Ferulic acid | 3 | 66.76 |
| Muramic acid | 4 | 142.47 |
| trans-Aconitic acid | 4 | 111.9 |
| Adipic acid | 5 | 74.6 |
| Chlorogenic acid | 5 | 164.75 |
| Citric acid | 5 | 132.13 |
| Propiomazine | 5 | 48.85 |
| Rutin | 6 | 269.43 |
| (E)-parinaric acid | 12 | 37.3 |
| α-Eleostearic acid | 13 | 37.3 |

The ADME analysis results of the compounds are shown in the table 4.3. The 33 compounds did not show any adverse effect in every parametres. The toxicity profile also showed acceptable results for them in the table (4.3).

**Table4.3 ADME Evaluation of phytochemicals**

| Name | GI absorptio | BBB permeant | Pgp substrate | CYP1A2 inhibitor | CYP2C19 inhibitor | CYP2C9 inhibitor | CYP2D6 inhibitor | CYP3A4 inhibitor | Bioavailability Score |
|---|---|---|---|---|---|---|---|---|---|
| (±)-Malic Acid | High | No | No | No | No | No | No | No | 0.56 |
| (E)-parinaric acid | High | Yes | No | Yes | No | Yes | No | No | 0.85 |
| 4-Hydroxycoumarin | High | Yes | No | Yes | No | No | No | No | 0.55 |
| 4-trifluoromethylmandelic acid | High | Yes | No | No | No | No | No | No | 0.85 |
| Adipic acid | High | No | No | No | No | No | No | No | 0.85 |
| Arecoline | High | No | No | No | No | No | No | No | 0.55 |
| Asiatic acid | High | No | Yes | No | No | No | No | No | 0.56 |
| Caffeic acid | High | No | No | No | No | No | No | No | 0.56 |
| Chlorogenic acid | Low | No | No | No | No | No | No | No | 0.11 |

| Maslinic acid | Linamarin | L-Aspartic acid | Kojic acid | Hederagenin | Gallic acid | Furaneol | D-(-)-Quinic acid | Citric acid | citramalic acid | **Name** |
|---|---|---|---|---|---|---|---|---|---|---|
| High | Low | High | High | High | High | High | Low | Low | High | **GI absorptio** |
| No | No | No | No | No | No | Yes | No | No | No | **BBB permeant** |
| Yes | Yes | No | No | Yes | No | No | No | No | No | **Pgp substrate** |
| No | No | No | No | No | No | No | No | No | No | **CYP1A2 inhibitor** |
| No | No | No | No | No | No | No | No | No | No | **CYP2C19 inhibitor** |
| No | No | No | No | No | No | No | No | No | No | **CYP2C9 inhibitor** |
| No | No | No | No | No | No | No | No | No | No | **CYP2D6 inhibitor** |
| No | No | No | No | No | Yes | No | No | No | No | **CYP3A4 inhibitor** |
| 0.56 | 0.55 | 0.56 | 0.55 | 0.56 | 0.56 | 0.85 | 0.56 | 0.56 | 0.56 | **Bioavailability Score** |

| Ellagic acid | Kaempferol | α-Eleostearic acid | trans-Aconitic acid | Succinic acid | propiomazine | Pipecolic acid | Oleanolic acid | Nicotinic acid | Muramic acid | **Name** |
|---|---|---|---|---|---|---|---|---|---|---|
| High | High | High | High | High | High | High | Low | High | Low | **GI absorptio** |
| No | No | Yes | No | No | Yes | No | No | Yes | No | **BBB permeant** |
| No | No | No | No | No | No | No | No | No | Yes | **Pgp substrate** |
| Yes | Yes | Yes | No | No | No | No | No | No | No | **CYP1A2 inhibitor** |
| No | No | No | No | No | No | No | No | No | No | **CYP2C19 inhibitor** |
| No | No | Yes | No | No | Yes | No | No | No | No | **CYP2C9 inhibitor** |
| No | Yes | No | No | No | Yes | No | No | No | No | **CYP2D6 inhibitor** |
| No | Yes | No | No | No | Yes | No | No | No | No | **CYP3A4 inhibitor** |
| 0.55 | 0.55 | 0.85 | 0.56 | 0.85 | 0.55 | 0.55 | 0.85 | 0.85 | 0.55 | **Bioavailability Score** |

| Name | GI absorptio | BBB permeant | Pgp substrate | CYP1A2 inhibitor | CYP2C19 inhibitor | CYP2C9 inhibitor | CYP2D6 inhibitor | CYP3A4 inhibitor | Bioavailability Score |
|---|---|---|---|---|---|---|---|---|---|
| Rutin | Low | No | Yes | No | No | No | No | No | 0.57 |
| Coumarin | High | Yes | No | Yes | No | No | No | No | 0.55 |
| Syringic acid | High | No | No | No | No | No | No | No | 0.56 |
| Ferulic acid | High | Yes | No | No | No | No | No | No | 0.85 |
| Ursolic acid | Low | No | No | No | No | No | No | No | 0.85 |

**Table4.4 Toxicity Evaluation**

| | Ames mutagenesis | Human Intestinal Absorption | Acute Oral Toxicity (mg/kg) | Oral Rat Acute Toxicity (LD50) (mg/kg) | Hepato toxicity |
|---|---|---|---|---|---|
| **(±)-Malic Acid** | No | No | 1.16 | 1.56 | No |
| **(E)-parinaric acid** | No | Yes | 1.44 | 1.45 | Yes |
| **4-Hydroxycoumarin** | No | Yes | 1.31 | 2.15 | No |
| **4-trifluoromethylmandelic acid** | No | Yes | 2.70 | 2.58 | No |
| **Adipic acid** | No | Yes | 1.02 | 1.58 | No |
| **Arecoline** | Yes | Yes | 1.58 | 2.27 | No |
| **Asiatic acid** | No | Yes | 2.87 | 3.15 | Yes |
| **Caffeic acid** | No | Yes | 1.51 | 2.42 | No |
| **Chlorogenic acid** | No | Yes | 2.03 | 2.07 | Yes |
| **citramalic acid** | No | Yes | 1.22 | 1.60 | No |
| **Citric acid** | No | Yes | 3.47 | 1.89 | No |

| | | | | | |
|---|---|---|---|---|---|
| **D-(-)-Quinic acid** | No | No | 1.21 | 2.34 | No |
| **Furaneol** | No | Yes | 1.92 | 1.59 | No |
| **Gallic acid** | No | Yes | 1.58 | 2.03 | No |
| **Hederagenin** | No | Yes | 2.32 | 2.09 | No |
| **Kojic acid** | No | Yes | 2.90 | 2.86 | Yes |
| **L-Aspartic acid** | Yes | Yes | 1.54 | 2.12 | No |
| **Linamarin** | No | Yes | 1.61 | 1.64 | No |
| **Maslinic acid** | No | No | 2.87 | 2.77 | Yes |
| **Muramic acid** | No | No | 1.87 | 2.26 | No |
| **Nicotinic acid** | Yes | Yes | 1.83 | 1.91 | No |
| **Oleanolic acid** | No | Yes | 1.75 | 2.25 | No |
| **Pipecolic acid** | No | Yes | 2.92 | 1.90 | No |
| **propiomazine** | No | Yes | 1.08 | 2.94 | Yes |
| **Succinic acid** | No | Yes | 2.15 | 1.75 | No |
| **trans-Aconitic acid** | No | Yes | 1.53 | 1.86 | No |
| **Ursolic acid** | No | Yes | 1.67 | 2.30 | Yes |
| **α-Eleostearic acid** | No | Yes | 2.83 | 1.44 | No |
| **Kaempferol** | No | Yes | 1.54 | 2.20 | No |
| **Ellagic acid** | No | Yes | 1.72 | 2.39 | No |
| **Rutin** | Yes | Yes | 2.29 | 2.49 | No |
| **Coumarin** | Yes | Yes | 1.62 | 2.04 | No |
| **Syringic acid** | No | Yes | 2.41 | 2.16 | No |
| **Ferulic acid** | No | Yes | 1.44 | 2.28 | No |

### 4.3.3 Protein structure retrieval:

Forty four structures of TNF-α obtained by both X-ray diffraction and solution NMR method with different resolutions are available; among them, a crystal structure with a resolution of 2.10 Å (PDB ID: 2AZ5) was selected. Its sequence length is 148 amino acids and the structure is non-mutated. For IL1β, 58 structures are available on RCSB PDB. The selected crystal structure among them has a resolution of 1.27 Å, 153 amino acids long sequence (5R7W). The third protein COX-2 (5F19) has a total of 7 structures available in RCSB PDB. From them, a structure with a sequence length of 552 amino acids determined in 2.04 Å X-ray diffraction method.

**Table4.5 Structure evaluation of proteins A) TNF-α, B) IL1β and C) COX-2**

**A)**

| PDB ID | Mutation | Missing residue no. | Resolution (Å) |
|---|---|---|---|
| 5UUI | Yes | NA | 1.40 |
| 4Y6O | No | 33 | 1.60 |
| 4TSV | Yes | NA | 1.80 |
| 2E7A | Yes | NA | 1.80 |
| 5M2J | No | 18 | 1.90 |
| **2AZ5** | **No** | **50** | **2.1** |
| 3L9J | No | 4 | 2.10 |
| 7JRA | No | 39 | 2.10 |
| 5M2I | No | 56 | 2.15 |
| 7KP9 | No | 56 | 2.15 |
| 7KPA | No | 48 | 2.30 |
| 5M2M | No | 55 | 2.30 |
| 1A8M | Yes | NA | 2.30 |
| 7TA3 | No | 25 | 2.50 |
| 6OOY | No | 57 | 2.50 |
| 5TSW | Yes | NA | 2.50 |
| 2ZJC | Yes | NA | 2.50 |
| 6OP0 | No | 67 | 2.55 |
| 4G3Y | No | 15 | 2.6 |
| 1TNF | No | 15 | 2.60 |
| 6RMJ | No | 53 | 2.65 |
| 7KP7 | Yes | NA | 2.65 |
| 7TA6 | No | 168 | 2.67 |
| 5YOY | No | 202 | 2.73 |
| 6X82 | No | 105 | 2.75 |
| 6OOZ | No | 57 | 2.80 |
| 3IT8 | No | 204 | 2.80 |
| 6X81 | No | 96 | 2.81 |
| 6X83 | No | 139 | 2.83 |
| 2ZPX | Yes | NA | 2.83 |
| 4TWT | No | 65 | 2.85 |
| 6X85 | No | 106 | 2.85 |

| | | | |
|---|---|---|---|
| 5WUX | No | 117 | 2.90 |
| 6X86 | No | 104 | 2.93 |
| 5MU8 | No | 677 | 3.00 |
| 7KPB | Yes | NA | 3.00 |
| 3ALQ | Yes | NA | 3.00 |
| 3WD5 | No | 10 | 3.10 |
| 2TUN | Yes | 36 | 3.10 |
| 7KP8 | Yes | NA | 3.15 |
| 7AT7 | Yes | NA | Solution NMR |
| 7ATB | Yes | NA | Solution NMR |
| 7QLF | Yes | NA | Solution NMR |
| 7ASY | No | NA | Solution NMR |

B)

| **PDB ID** | **Mutation** | **Missing residue no.** | **Resolution (Å)** |
|---|---|---|---|
| 5R8Q | No | 1 | 1.23 |
| **5R7W** | **No** | **1** | **1.27** |
| 5R8E | No | 1 | 1.35 |
| 5R8M | No | 1 | 1.39 |
| 5R8F | No | 1 | 1.41 |
| 5R8O | No | 1 | 1.42 |
| 5R8G | No | 1 | 1.43 |
| 5R85 | No | 1 | 1.44 |
| 6Y8I | No | 6 | 1.46 |
| 5R87 | No | 1 | 1.47 |
| 5R8A | No | 1 | 1.47 |
| 5R8D | No | 1 | 1.47 |
| 5R8I | No | 1 | 1.47 |
| 5R8K | No | 1 | 1.47 |
| 5R88 | No | 1 | 1.48 |
| 5R8N | No | 1 | 1.48 |
| 4GAI | No | 13 | 1.49 |
| 5R8B | No | 1 | 1.49 |
| 5R86 | No | 1 | 1.5 |

| | | | |
|---|---|---|---|
| 5R8H | No | 1 | 1.5 |
| 2NVH | No | 1 | 1.53 |
| 5R8P | No | 1 | 1.53 |
| 1L2H | Yes | NA | 1.54 |
| 5R8C | No | 1 | 1.54 |
| 5R8L | No | 1 | 1.56 |
| 5R8J | No | 1 | 1.62 |
| 5R89 | No | 1 | 1.65 |
| 3POK | Yes | NA | 1.7 |
| 6Y8M | No | 4 | 1.9 |
| 1I1B | No | 2 | 2 |
| 21BI | Yes | NA | 2 |
| 2I1B | No | NA | 2 |
| 31BI | Yes | NA | 2 |
| 4I1B | No | 2 | 2 |
| 4G6J | No | 9 | 2.03 |
| 1T4Q | Yes | NA | 2.1 |
| 1TOO | Yes | NA | 2.1 |
| 1TWE | Yes | NA | 2.1 |
| 3LTQ | No | 2 | 2.1 |
| 5I1B | No | 2 | 2.1 |
| 4GAF | No | 13 | 2.15 |
| 5MVZ | No | 14 | 2.15 |
| 1TP0 | Yes | NA | 2.2 |
| 5BVP | No | 10 | 2.2 |
| 1TWM | Yes | NA | 2.26 |
| 9ILB | No | 11 | 2.28 |
| 1S0L | Yes | NA | 2.34 |
| 1HIB | No | 3 | 2.4 |
| 1ITB | No | 0 | 2.5 |
| 7CHZ | No | 20 | 2.5 |
| 7CHY | No | 22 | 2.65 |
| 41BI | Yes | NA | 2.9 |
| 4DEP | No | 23 | 3.1 |
| 3O4O | No | 20 | 3.3 |
| 7Z4T | No | 12 | 3.3 |
| 2KH2 | No | NA | Solution NMR |
| 6I1B | No | NA | Solution NMR |
| 7I1B | No | NA | Solution NMR |

C)

| PDB ID | Mutation | Missing residue no. | Resolution (Å) |
|---|---|---|---|
| **5F19** | **No** | **14** | **2.04** |
| 5IKR | No | 7 | 2.342 |
| 5F1A | No | 5 | 2.38 |
| 5IKQ | No | 5 | 2.41 |
| 5IKT | No | 6 | 2.451 |
| 5IKV | No | 7 | 2.508 |
| 5KIR | No | 4 | 2.697 |

### 4.3.4 Sequence alignment and homology modeling:

The protein structures which were selected as the target proteins have missing residues and atoms. The 2AZ5 structure of TNF-α has 50 missing residues in its four chains. To prepare the structure for molecular docking studies, the chain which showed maximum interaction with ligands as explained in studies by previous authors, was taken for modelling. For 2AZ5, chain A was taken up which has 16 residues missing. Among the 7 structures listed for COX-2 in RCSB PDB databank, the 5F19 PDB structure was taken up. The structure has 14 missing residues altogether and selected chain B has 5 missing residues. For IL1β, the selected structure 5R7W got 7 missing residues in its only chain in the structure. The sequence of human Tumor necrosis factor α (TNF-α), Interleukin-1 β (IL1β) and Cyclooxygenase 2 (COX-2) with accession number P01375, P01584 and P35354 respectively were retrieved from UniProt and the structure was modeled by MODELLER.

### 4.3.5 Molecular docking studies:

This technique was carried out to computationally determine the binding site of Tumor necrosis factor α (TNFα), Interleukin-1 β (IL1β) and Cyclooxygenase 2 (COX-2), which aided in corroborating experimental findings. Docking run was performed with the ligand molecules after they have passed the “Lipinski’s Rule of Five” and “ADMET” properties. The ligands were allowed to interact with the active site residues of the protein molecule to predict the efficient inhibitor of the proteins. A grid configuration are given for 3 different proteins to be docked in table 4.6. With the help of Autodock Vina, thirty three docked conformers were generated for each

of the three proteins, each with its own respective binding energy. The molecules were screened on the basis of their docking score and its interaction with its active site residues. These results were used for the further analysis.

**Table4.6 Grid conformations for Molecular Docking Simulation**

| Conformations | Tumor necrosis factor α (TNF-α) | Interleukin-1 β (IL1β) | Cyclooxygenase 2 (COX-2) |
|---|---|---|---|
| Center of X | 1.491 | 76.241 | 53.041 |
| Center of Y | 34.314 | 53.874 | -30.125 |
| Center of Z | 1.065 | -4.579 | 64.682 |
| Size of X | 38 | 50 | 40 |
| Size of Y | 46 | 44 | 46 |
| Size of Z | 32 | 56 | 50 |

It can be observed from the Table 4.7, that most of the ligands target molecules could accommodate well in the active site pocket and had varied docking score (ΔG). For TNFα, IL1β and COX-2 the highest score came out to be -8.4, -8, -8.4kcal/mol and the lowest to be -4, -4.1, -4.3kcal/mol respectively. ΔG or the change in Gibbs free energy represents the spontaneous reaction of the reactants in an experiment where there is no requirement of external forces. Therefore, the negative values of the ΔG during the docking experiment represents that the reaction was spontaneous and is preferred for efficient binding. When docking with TNFα, for the polyphenols, ellagic acid and rutin was showing highest docking score of -6.6 kcal/mol followed by kaempferol (-6.5 kcal/mol) and chlorogenic acid (-6.4 kcal/mol). IL1β docking with phytochemicals also depicts highest score in ellagic acid (-7.6 kcal/mol) followed by rutin (-7.3 kcal/mol), kaempferol (-6.8 kcal/mol) and chlorogenic acid (-6.6 kcal/mol). The result of docking of COX-2 resulted in the highest docking score among the three target proteins of -8.4 kcal/mol followed by chlorogenic acid (-7.1 kcal/mol), kaempferol (-6.9 kcal/mol) and ellagic acid (-6.8 kcal/mol).

**Table4.7 Docking scores of ligands with target protein**

| **Compounds** | **Bonding energy (Kcal/mol)** | | |
|---|---|---|---|
| | **Interleukin-1 β (IL1β)** | **Tumor necrosis factor α (TNF-α)** | **Cyclooxygenase 2 (COX-2)** |
| Maslinic acid | -8 | -8.4 | -8 |
| Ursolic acid | -7.9 | -8 | -7 |
| Oleanolic acid | -7.9 | -7.8 | -7.2 |
| Hederagenin | -7.6 | -7.4 | -7.1 |
| Asiatic acid | -7.4 | -6.8 | -6.9 |
| Ellagic acid | -7.6 | -6.6 | -6.8 |
| Rutin | -7.3 | -6.6 | -8.4 |
| Kaempferol | -6.8 | -6.5 | -6.9 |
| Chlorogenic acid | -6.6 | -6.4 | -7.1 |
| propiomazine | -5.5 | -5.7 | -5.8 |
| Coumarin | -4.9 | -5.7 | -5.5 |
| 4-Hydroxycoumarin | -5.5 | -5.6 | -5.6 |
| 4-trifluoromethylmandelic acid | -5.4 | -5.3 | -5.7 |
| Gallic acid | -5.4 | -5.3 | -5.2 |
| Caffeic acid | -5.1 | -5.3 | -5.5 |
| D-(-)-Quinic acid | -5.5 | -5.2 | -5.3 |
| Muramic acid | -6 | -5.1 | -5.4 |
| Ferulic acid | -5.1 | -5 | -5.3 |
| trans-Aconitic acid | -4.8 | -5 | -5.2 |
| (E)-parinaric acid | -4.2 | -5 | -5.5 |
| Syringic acid | -5.3 | -4.9 | -5 |
| Linamarin | -5.7 | -4.8 | -5.1 |
| Citric acid | -5 | -4.8 | -4.7 |
| Nicotinic acid | -4.5 | -4.7 | -4.3 |
| Pipecolic acid | -4.6 | -4.6 | -4.7 |

| | | | |
|---|---|---|---|
| Kojic acid | -4.9 | -4.5 | -4.8 |
| Succinic acid | -4.1 | -4.5 | -4.4 |
| citramalic acid | -4.6 | -4.4 | -4.8 |
| Arecoline | -4.2 | -4.3 | -4.3 |
| Adipic acid | -4.1 | -4.3 | -4.3 |
| Furaneol | -4.3 | -4.2 | -4.6 |
| L-Aspartic acid | -4.5 | -4.1 | -5 |
| (±)-Malic Acid | -4.5 | -4 | -4.9 |

To reevaluate the docking interactions having highest scores we docked the top phytochemicals again with the target proteins by a webserver called swissdock. The docking resulted the best score for rutin when docked against all three target proteins and the results are presented in table 4.8. Analyzing results both from autodock and swissdock, rutin turned out to be the best compound to target the anti-inflammatory marker proteins we are following for the study. So after checking the docked complexes for its interaction comparing between autodock and swissdock, it is further taken for the next process of molecular dynamic simulation. The analysis of this comparison are presented in the table (4.8).

**Table4.8 Bonding energy during Docking by swissdock**

| **Docked complexes** | **Bonding energy (Kcal/mol)** | **docked complexes** | **Bonding energy (Kcal/mol)** | **docked complexes** | **Bonding energy (Kcal/mol)** |
|---|---|---|---|---|---|
| TNFα-rutin | -8.59 | IL1β-rutin | -7.91 | COX-2-rutin | -8.61 |
| TNFα-ellagic acid | -7.53 | IL1β-chlorogenic acid | -7.82 | COX-2-ellagic acid | -7.76 |
| TNFα-chlorogenic acid | -7.04 | IL1β-ellagic acid | -7.72 | COX-2-chlorogenic acid | -7.19 |
| TNFα-kaempferol | -6.75 | IL1β-kaempferol | -6.44 | COX-2-kaempferol | -7.08 |

**Table4.9 Bond lengths during Docking by swissdock**

| Swissdock | | | | | | | | |
|---|---|---|---|---|---|---|---|---|
| **TNFα_Rutin** | | | **IL1β_Rutin** | | | **COX-2-Rutin** | | |
| **Bonding residue** | **Bond length** | **Bond type** | **Bonding residue** | **Bond length** | **Bond type** | **Bonding residue** | **Bond length** | **Bond type** |
| Ala75 | 5.19 | Alkyl | Pro2 | 1.97 | H-bond | Leu193 | 4.82 | Pi |
| Val76 | 4.88 | Alkyl | | 2.47 | Metal accepter | Asp198 | 3.02 | H-bond |
| | 2.65 | H-bond | Ser5 | 1.91 | H-bond | | | |
| Val82 | 5.07 | Alkyl | Asn7 | 2.92 | Metal accepter | | | |
| | 4.22 | Alkyl | Glu64 | 4.54 | Pi | | | |
| Lys119 | 1.79 | H-bond | Ser153 | 4.84 | Pi | | | |
| | | | | 3.64 | Pi | | | |
| **Total no. of bonds** | 6 | | **Total no. of bonds** | 7 | | **Total no. of bonds** | 2 | |

**Table4.10 Docking by Autodock**

| Autodock | | | | | | | | |
|---|---|---|---|---|---|---|---|---|
| **COX-2-Rutin** | | | **IL1B-Rutin** | | | **TNF-Rutin** | | |
| **Bonding residue** | **Bond length** | **Bond type** | **Bonding residue** | **Bond length** | **Bond type** | **Bonding residue** | **Bond length** | **Bond type** |
| trp19 | 1.82 | H-bond | Ser5 | 2.65 | H-bond | Trp19 | 1.82 | H-bond |
| asn37 | 2.83 | Pi | Asn7 | 2.41 | H-bond | Asn37 | 2.32 | H-bond |
| | 2.32 | H-bond | | 2.03 | H-bond | | 2.83 | Pi |
| gln38 | 2.8 | H-bond | Ser43 | 2.1 | H-bond | Gln38 | 2.8 | H-bond |
| lys81 | 2.01 | H-bond | | 2.58 | H-bond | Lys81 | 2.01 | H-bond |
| glu126 | 2.83 | H-bond | Leu62 | 3 | H-bond | Glu126 | 2.83 | H-bond |
| | 4.15 | Pi | Glu64 | 2.84 | H-bond | | 4.83 | Pi |
| | 4.18 | Pi | | 4.73 | Pi | | 4.15 | Pi |
| | | | Lys65 | 2.12 | H-bond | | | |
| | | | Asn66 | 2.45 | H-bond | | | |
| | | | Pro87 | 2.03 | H-bond | | | |
| | | | Ser153 | 2.44 | H-bond | | | |
| Total no. of bonds | 8 | | Total no. of bonds | 12 | | Total no. of bonds | 8 | |

### 4.3.6 Molecular dynamics simulation:

Investigating protein-ligand interactions makes use of the potent techniques of molecular docking and molecular dynamics (MD). While MD can be used to include flexibility into docking calculations and obtain additional information on the kinetics and stability of the protein-ligand bond, molecular docking tools predict the binding posture and affinity of a protein-ligand complex. Recent years have seen a significant increase in the application of molecular dynamic (MD) simulation for a better understanding of the structure, mutation, dynamic behavior of protein and protein– ligand interaction. The time-dependent behavior of a system is precisely recorded by this simulation analysis. The actual movements of atoms and molecules are examined in MD simulation. The atoms and molecules are let to interact for a set period of time, giving rise to a glimpse of the dynamic "evolution" of the system. The position of atoms, along with the energy function of the system are known. In the MD simulation Newtonian mechanics has been implemented to estimate the forces that are acting at the respective atoms. This computational method can be used to appropriately evaluate the roles of macromolecules and complexes based on dynamics, structure, and thermodynamics. The protein's structure and its dynamics both in the absence and presence of the ligand, are best defined mainly by MD simulations. According to prior studies, this type of technique is frequently used in the drug designing field to predict the drug target structure and support study findings.

An essential feature to track the system's process of equilibrium and the stability of the protein structure upon ligand binding is the root mean square deviation (RMSD) of the protein structure as a function of time [42]. The RMSD is utilized in MD simulation to evaluate structural departure from the starting protein structure [43]. The residue was assessed to examine the flexibility of its protein, ligand and their complexes. Calculation of root mean square deviation (RMSD) was carried out between the initial structures and simulated structures for the systems that were studied. The RMSD value gives us the information of the local dynamics of the studied protein structure and also in understanding the behavior of the protein structures during the simulation period. The movements of the atoms were studied during the MD simulation runs which indicate that higher and lower RMSD values showed higher and lower movements of atoms respectively.

We calculated the RMSD values for the whole simulation trajectories that included the non-hydrogen atoms of the molecules. The conformations with the lowest energy score of docking were chosen for the final production run of the MD simulation in order to better understand the dynamics of the protein–ligand complexes and the stability of the protein. Two different scenarios for each of three target proteins (TNFα, IL1β and COX-2) were investigated that are different from each other, involving a target protein (ligand unbound) in water as a control, and another was the target protein bound with the ligand (rutin) and the results are represented in fig. 4.2 respectively. Comparison between the RMSD values of the structure that underwent simulations showed that the complexes reached its equilibrium during the early simulation cycle in comparison to its control protein. Trajectory analysis was used to investigate the dynamic nature, including root mean square deviation (RMSD), root mean square fluctuation (RMSF), and also the radius of gyration (Rg).The RMSD of the protein and the complex is shown in Fig.4.2 The unboundTNFα-RMSD graph (a) showed a rise in fluctuation from the start, and the first peak of approximately 0.34 nm at 15 ns was observed. Subsequently, it exhibited similar range peaks till ~38 ns and eventually attained a stable state from there. In the presence of rutin, the RMSD plot of the complex varied more in comparison to the RMSD plot of unbound protein. This occurred as a result of the ligand attempting to create a stronger binding with TNFα. In the case of rutin-TNFα simulated in a water box, the RMSD graph appeared conserved from around 67ns to 77ns and again from 85 ns to 92 ns before being unstable again. The largest fluctuation peaked at0.45 nm around 67 ns, and its RMSD value was much larger than the protein after 43 ns throughout the whole simulation's100 ns duration. The higher RMSD value observed for the protein-ligand complexed state indicated larger conformational changes in the protein due to ligand association ultimately trying to attain stability. The RMSD plot of the IL1β-rutin with respect to IL1β native protein shows similar pattern throughout the simulation. The IL1β-rutin bound structure was showing less RMSD values than the simulation of native protein structure in water till 30 ns and a gradual increase later on.The COX-2 protein and complex COX-2-rutin stability during simulation are shown by root mean square deviation (RMSD) plot in fig.4.2. The first peak can be seen at 9 ns of 0.34 n height. The ligand bound COX-2 showed enhanced stability maneuvering in higher RMSD value in a fairly stable graph from 12 ns to 100ns. It depicts a stronger bond between COX-2 and ligand.

a)

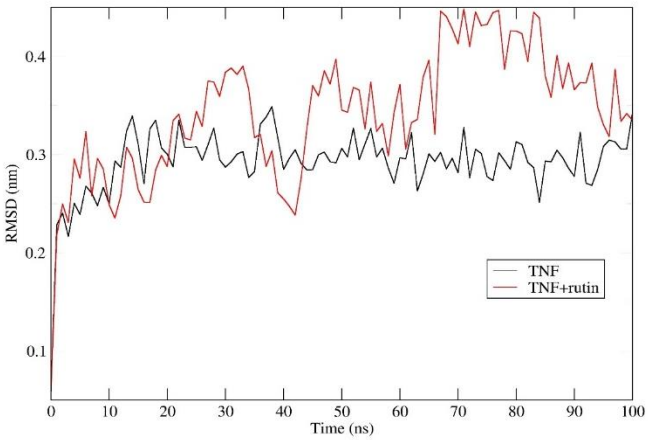


b)

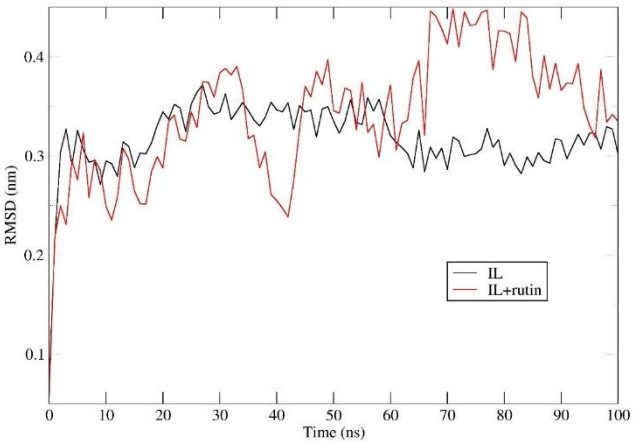


c)

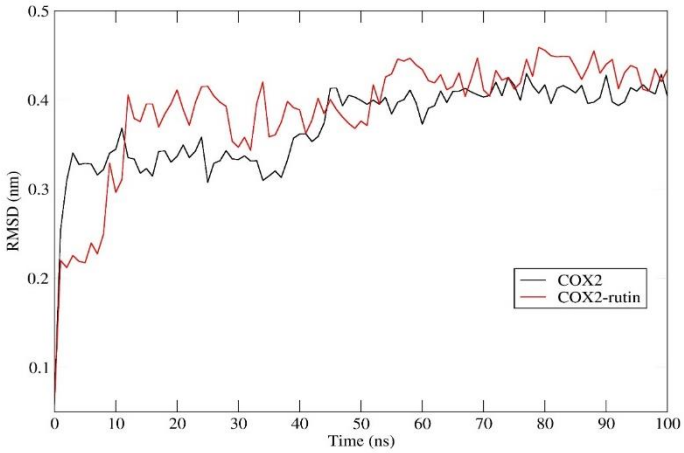


**Fig.4.2 RMSD of a) TNFα and complex TNFα-rutin, (b) IL1β and complex IL1β-rutin, (c) COX-2 and complex COX-2-rutin**

To better comprehend residue-by-residue changes over timeof a protein, we observed root-mean-square fluctuations(RMSF). The RMSF analysis detects residue variations, which are crucial since any major changes in the flexibility of functionally important residues would have an effect on the target protein function. To account for residue level fluctuation-based changes during the MD simulation, RMSF analysis was used. For all three target proteins, TNFα,IL1β and COX-2 the ligand-bound environments practically exhibited a similar fluctuation trend with their native unbound protein structure, as displayed in Fig.4.3 When we travel through the RMSF, we observe that for both TNFα and COX-2 bound with ligand complexes, a lot of residues also overlap with

their native proteins. Based on this, it may be concluded from the overlapped fluctuations of the two complexes (rutin-TNFα and rutin-COX-2), the protein flexibility was not impacted after the ligands were bound. A little more variability was present in ligand-bounded protein than in ligand-unbounded protein. Regional variations are fewer, which implies that these regions are less versatile. Large variation in IL1β-rutin complex shows a less stable structure compared to the other two.

a) b)

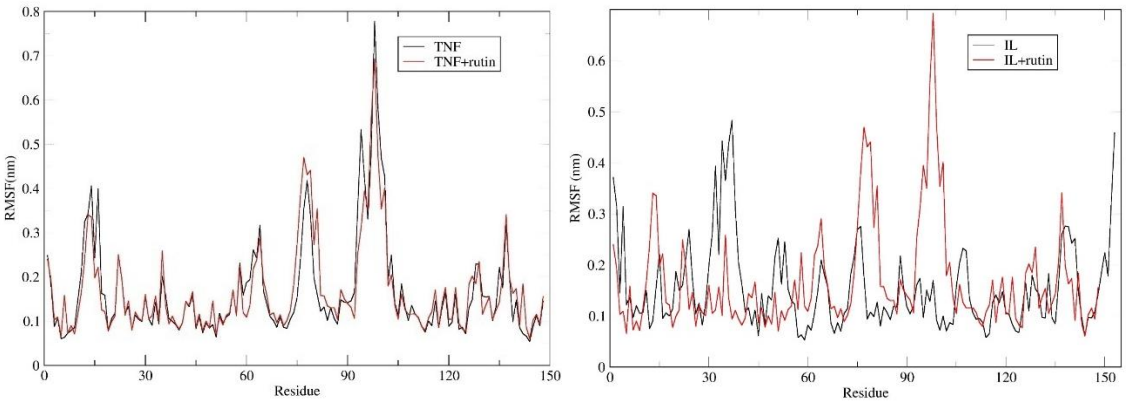


c)

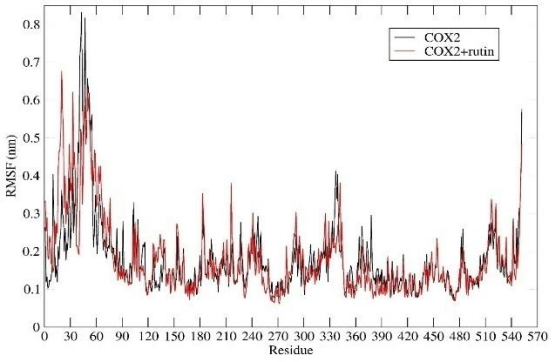


**Fig.4.3 RMSF of a) TNFα and complex TNFα-rutin, (b) IL1β and complex IL1β-rutin, (c) COX-2 and complex COX-2-rutin**

Another parameter that determines the structural dynamics of proteins is the radius of gyration (Rg). The rigidity of the complex is determined by the intermolecular forces of attraction between the ligand and protein, with a strong force of interaction indicating a very compact complex and vice versa. Thus, by measuring the Rg, the degree of compactness of the receptor

protein with its ligands determines its tight binding and the measurement of the hydrodynamic diameter of the structures were done. The radius of gyration for the structures were plotted as the simulation period against time. From Fig.4.4 it could be seen that throughout the simulation time TNFα and COX-2 showed essentially similar range of Rg values while the ligand was present and also in its absence. Rutin bound TNFα displayed more compactness than the control protein after 66 ns and it continued till the ending of 100 ns. COX-2 with ligand showed similar range and almost constantly overlapped plot from 65 ns till the ending. These results are in line with the RMSD plots of the complexes. The IL1β-rutin complex shows a significant difference and no overlapping of Rg plots with unbound IL1β. This result can be connected with RMSD and RMSF results being unstable for the protein complex.

a)

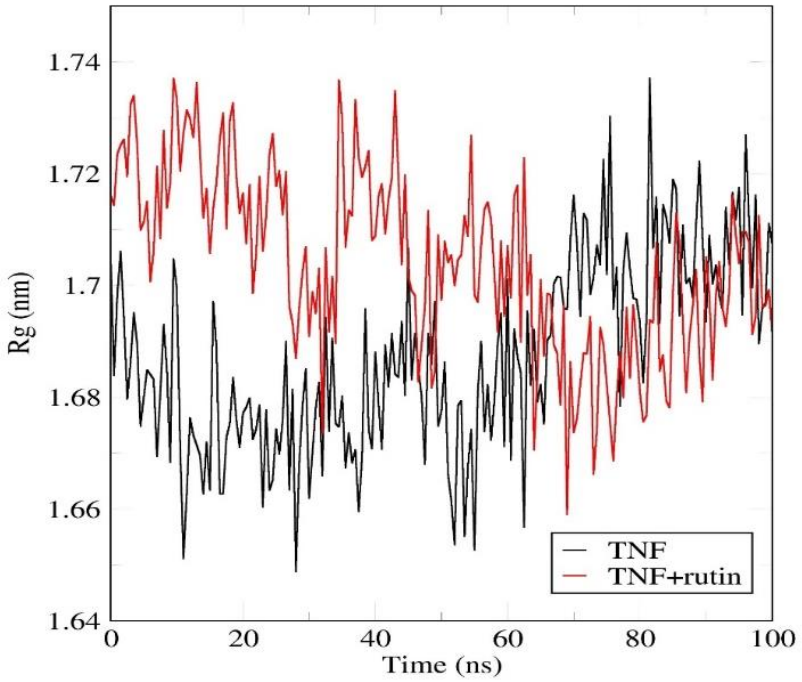

b)

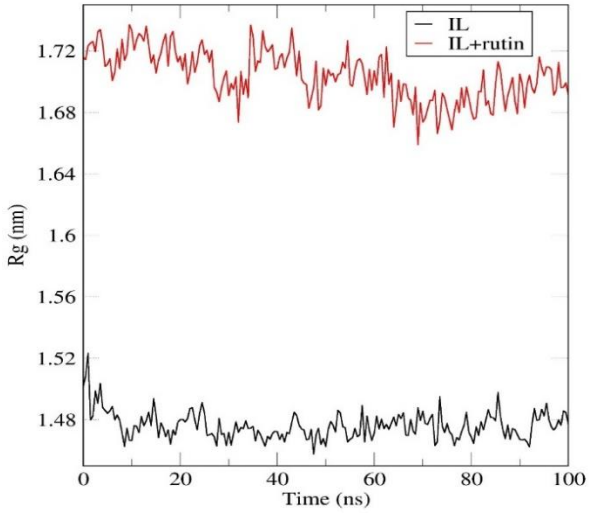


c)

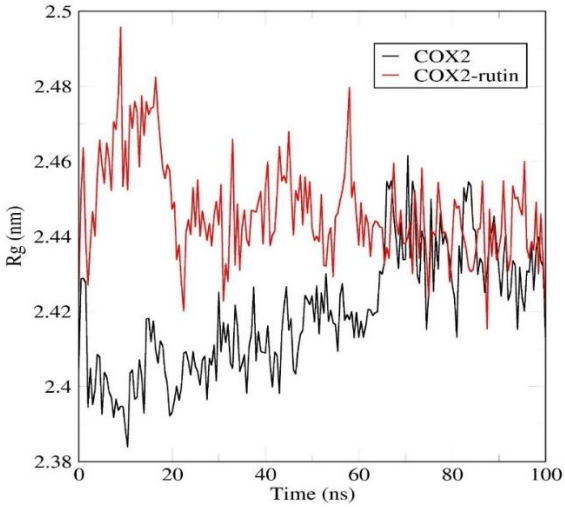


**Fig.4.4 Rg of a) TNFα and complex TNFα-rutin, (b) IL1β and complex IL1β-rutin, (c) COX-2 and complex COX-2-rutin**

The non-bonded interactions during the simulation of the docked complexes at 0, 50 and 100 ns are depicted in the Figure 4.4 and also tabulated the no. of interactions (table 4.11). It can be seen that for both the TNFα-rutin and IL1β-rutin protein-ligand complexes, the total no. of interactions increases from 0 to 100ns. But in case of COX-2-rutin, the no. increases from 0 to 50 ns and maintains the same total no. of bonds, indicating stability from 50 ns onwards.

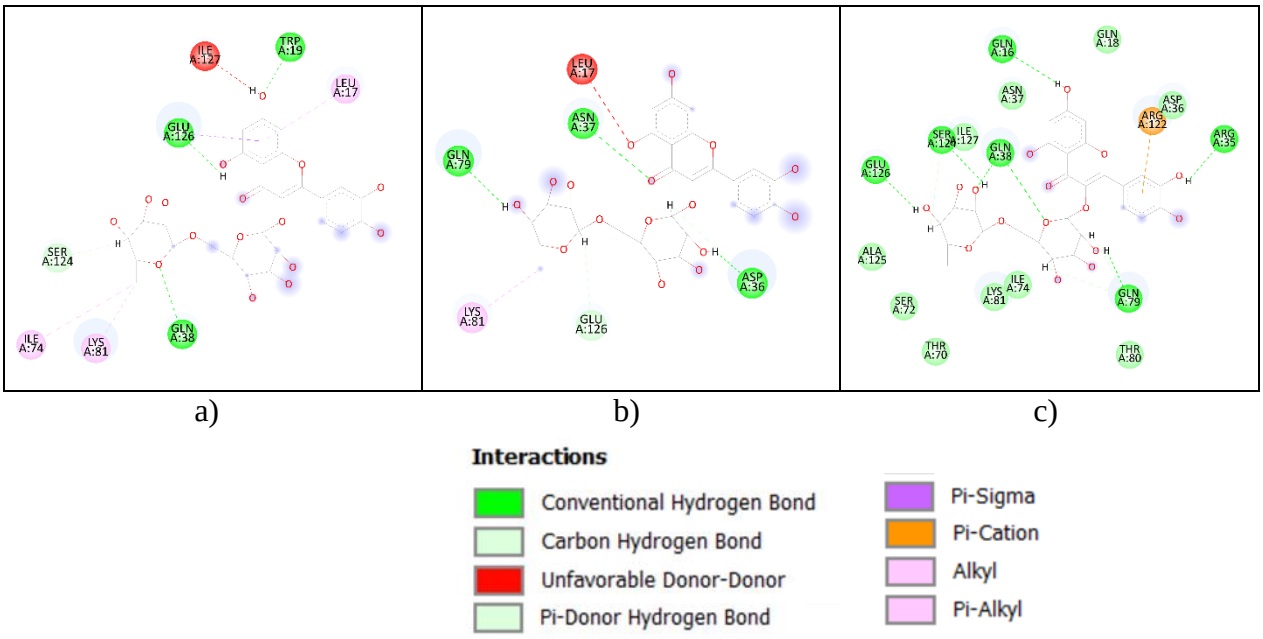


**Fig.4.5 2D-Interaction plot of TNFα-rutin at three time steps (a) 0, (b) 50 and (c) 100 ns respectively**

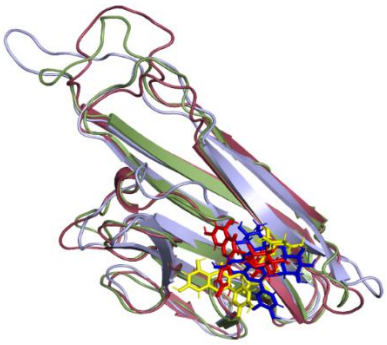

**Fig.4.6 complex TNFα-rutin at three time steps 0, 50 and 100 ns represented by colour light blue-red, green- yellow, raspberry – deep blue**

**Table4.11 The distributed non-bonded interactions numbers between the TNFα and the ligand rutin were counted throughout the entire simulation period**

| Protein-ligand | Time (ns) | Non-bonded interactions | | | | | | | | | Total no of interaction |
|---|---|---|---|---|---|---|---|---|---|---|---|
| | | Conventional H-bond | Pi-Donor H-bond | Van der Waals | Pi-alkyl | Alkyl | Pi - Cation | Carbon – H bond | Unfavorable Donor-Donor | Unfavorable Acceptor-Acceptor | |
| TNFα-rutin complex | 0 | 3 | 0 | 0 | 0 | 3 | 0 | 1 | 1 | 0 | 8 |
| | 50 | 3 | 0 | 0 | 0 | 1 | 0 | 1 | 0 | 1 | 6 |
| | 100 | 6 | 0 | 9 | 0 | 0 | 1 | 1 | 0 | 0 | 17 |

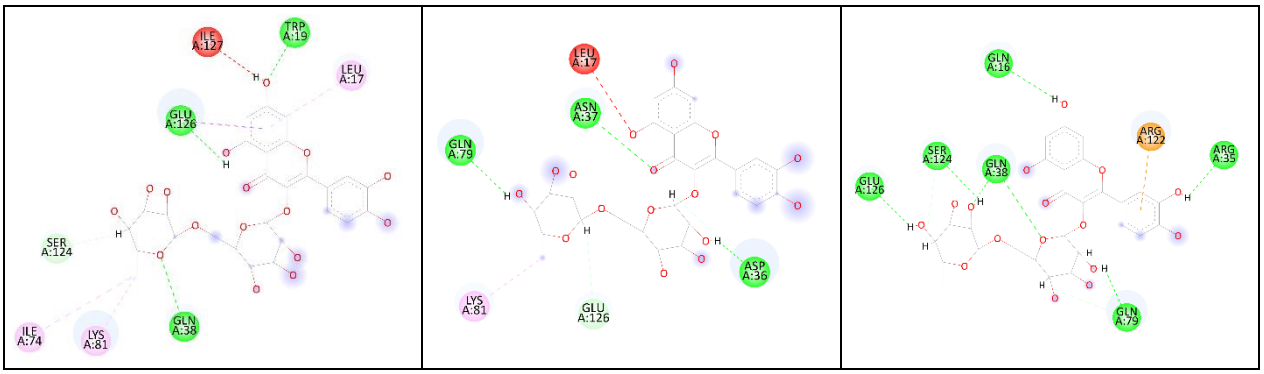


a) b) c)

**Fig.4.7 2D-Interaction plot of IL1β-rutin at three time steps (a) 0, (b) 50 and (c) 100 ns respectively**

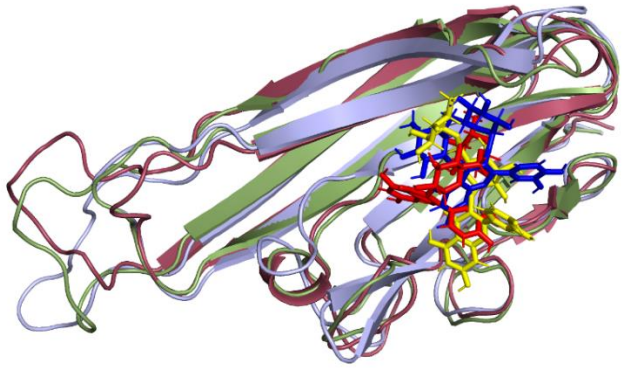

**Fig.4.8 Complex IL1β-rutin at three time steps 0, 50 and 100 ns represented by colour light blue-red, green- yellow, raspberry – deep blue**

**Table4.12 The distributed non-bonded interactions numbers between the IL1β and the ligand rutin were counted throughout the entire simulation period**

| Protein-ligand | Time (ns) | Non-bonded interactions | | | | | | | | | Total no of interaction |
|---|---|---|---|---|---|---|---|---|---|---|---|
| | | H-bond | Pi-Donor H-bond | Pi-Sigma | Pi-alkyl | Alkyl | Pi - Cation | Carbon – H bond | Unfavorable Donor-Donor | Unfavorable Acceptor-Acceptor | |
| IL1β-rutin complex | 0 | 3 | 0 | 0 | 0 | 3 | 0 | 1 | 1 | 0 | 8 |
| | 50 | 3 | 0 | 0 | 0 | 1 | 0 | 1 | 0 | 1 | 6 |
| | 100 | 4 | 0 | 0 | 1 | 0 | 0 | 4 | 0 | 0 | 9 |

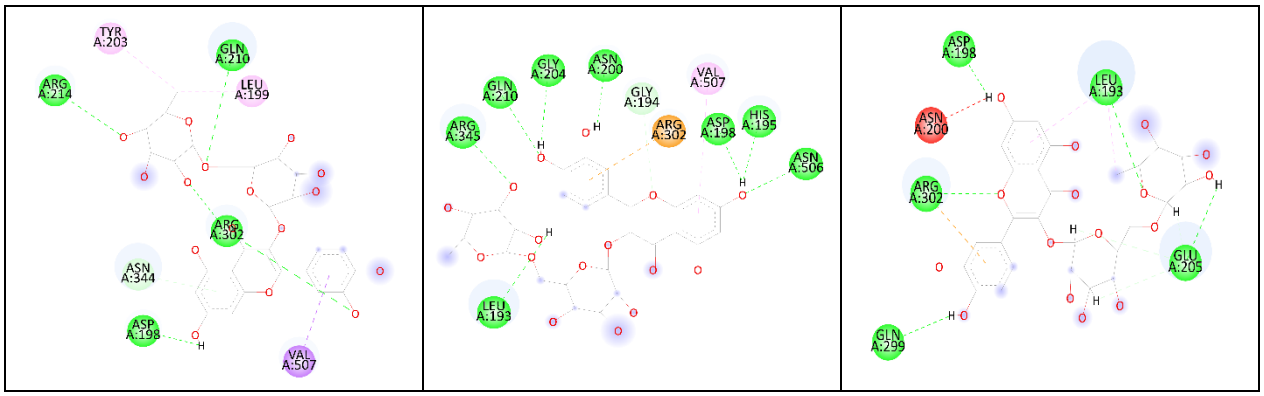


a) b) c)

**Fig.4.9 2D-Interaction plot of COX2-rutin at three timesteps (a) 0, (b) 50 and (c) 100 ns respectively**

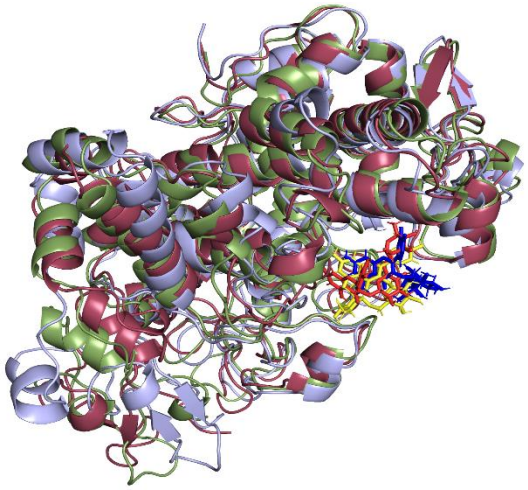

**Fig.4.10 complex COX2-rutin at three timesteps 0, 50 and 100 ns represented by colour light blue-red, green- yellow, raspberry – deep blue**

**Table4.13 The distributed non-bonded interactions numbers between the COX2 and the ligand rutin were counted throughout the entire simulation period**

| Protein-ligand | Time (ns) | Non-bonded interactions | | | | | | | | Total no of interaction |
|---|---|---|---|---|---|---|---|---|---|---|
| | | Conventional H-bond | Pi-Donor H-bond | Pi-Sigma | Pi-alkyl bond | Alkyl bond | Pi - Cation bond | Carbon –H bond | Unfavorable Donor-Donor | |
| COX2-rutin complex | 0 | 4 | 1 | 1 | 1 | 1 | 0 | 0 | 0 | 8 |
| | 50 | 8 | 0 | 0 | 1 | 0 | 1 | 1 | 0 | 11 |
| | 100 | 7 | 0 | 0 | 0 | 1 | 0 | 0 | 3 | 11 |

## 4.4 Conclusions

In the pharmaceutical industry, computational techniques are used widely in the process of development of drugs in order to reduce time consumption and money consumption. Therefore, in this present study, an initial step for development of potential inhibitors could be used for development of drugs. Various computational techniques such as molecular docking and molecular dynamic simulations were used to understand the structural changes and the dynamics of the protein-ligand complex. Rutin present in norabogori also exits in various medicinal plants and was used as natural inhibitor for potential inhibition of TNFα, IL1β and COX-2 inflammatory target protein and found them most promising to be used as an alternative in the development of drugs. Molecular dynamics simulation studies were executed to understand the dynamics of the natural molecule as inhibitors. They also play crucial role in understanding binding the natural molecules as inhibitors to the active site residues of the protein. Inhibition of prolyl hydroxylase and angiotensin converting enzyme opens up avenues for research and development of drugs.

## References


[1] Ben Hammouda, M., Ahmad, I., Hamdi, A., Dbeibia, A., Patel, H. M., Bouali, N., Sabri Hamadou, W., Hosni, K., Ghannay, S., Alminderej, F. M., Noumi, E., Snoussi, M., Aouadi, K., and Kadri, A. Design, synthesis, biological evaluation and *in silico* studies of novel 1,2,3-triazole linked benzoxazine-2,4-dione conjugates as potent antimicrobial, antioxidant and anti-inflammatory agents. *Arabian Journal of Chemistry*, 2022.

[2] El-Shwiniy, W. H., El-Desoky, S. I., Alrabie, A., and Abd El-wahaab, B. Spectrophotometric determination of Zr(IV), Hg(II) and U(VI) in solution with their analytical applications: Structural characterization and molecular docking of the solid complexes. *Spectrochimica acta. Part A, Molecular and biomolecular spectroscopy*, 279: 121400, 2022.

[3] Adhreai, A. A., AlSaeedy, M., Farooqui, M., and Al-Timari, U. Stereoselective Synthesis of Novel Chiral Open-Chain D-Ribose and D-Glucose- Derived Nitrones through 1,3-Dipolar Cycloaddition of Maleimide and Maleic Acid and Investigation of Their Antimicrobial Activity Via Molecular Docking and ADMET studies. *Journal of Molecular Structure*, 2022.

[4] Abdellatif, K. R. A., Abdelall, E. K. A., Elshemy, H. A. H., Lamie, P. F., El-Nahaas, E.-S., and Amin, D. M. E. Design, synthesis of new anti-inflammatory agents with a pyrazole core: COX-1/COX-2 inhibition assays, anti-inflammatory, ulcerogenic, histopathological, molecular Modeling, and ADME studies. *Journal of Molecular Structure*, 1240: 130554, 2021.

[5] Ghabi, A., Brahmi, J., Alminderej, F. M., Messaoudi, S., Vidal, S., Kadri, A., and Aouadi, K. Multifunctional isoxazolidine derivatives as α-amylase and α-glucosidase inhibitors. *Bioorganic chemistry*, 98: 103713, 2020.

[6] Partridge, K. M., Anzovino, M. E., and Yoon, T. P. Cycloadditions of N-sulfonyl nitrones generated by lewis acid catalyzed rearrangement of oxaziridines. *Journal of the American Chemical Society*, 130 10: 2920-2921, 2008.
[7] Nishiuchi, M., Sato, H., Umemoto, N., and Murakami, S. Exo Selective Cycloaddition Reactions of α-Hydroxy Cyclic Nitronates to Allylic Alcohols in the Presence of Magnesium Ions Leading to Isoxazolidines and Isoxazolines. *Chemistry Letters*, 37: 146-147, 2008.
[8] Ju, Z., Li, M., Xu, J., Howell, D. C., Li, Z., and Chen, F.-E. J. A. P. S. B. Recent development on COX-2 inhibitors as promising anti-inflammatory agents: The past 10 years. 12(6): 2790-2807, 2022.
[9] Kim, H. P., Son, K. H., Chang, H. W., and Kang, S. S. J. J. o. p. s. Anti-inflammatory plant flavonoids and cellular action mechanisms. 96(3): 229-245, 2004.
[10] García-Lafuente, A., Guillamón, E., Villares, A., Rostagno, M. A., and Martínez, J. A. J. I. r. Flavonoids as anti-inflammatory agents: implications in cancer and cardiovascular disease. 58(9): 537-552, 2009.
[11] Tona, L., Kambu, K., Ngimbi, N., Cimanga, K., and Vlietinck, A. J. J. o. e. Antiamoebic and phytochemical screening of some Congolese medicinal plants. 61(1): 57-65, 1998.
[12] Karmegam, N., Jayakumar, M., and Karuppusamy, S. J. J. o. p. s. Synergistic antibacterial activity of four medicinal plants collected from Dharapuram Taluk of Tiruppur District, south India. 7(1): 32, 2012.
[13] Ahmad, I. and Beg, A. Z. J. J. o. e. Antimicrobial and phytochemical studies on 45 Indian medicinal plants against multi-drug resistant human pathogens. 74(2): 113-123, 2001.
[14] Razack, S., Hemanth Kumar, K., Nallamuthu, I., Naika, M., and Khanum, F. J. A. Antioxidant, biomolecule oxidation protective activities of Nardostachys jatamansi DC and its phytochemical analysis by RP-HPLC and GC-MS. 4(1): 185-203, 2015.
[15] Loza-Mejía, M. A., Salazar, J. R., and Sánchez-Tejeda, J. F. J. B. *In silico* studies on compounds derived from Calceolaria: Phenylethanoid glycosides as potential multitarget inhibitors for the development of pesticides. 8(4): 121, 2018.
[16] Lee, K. and Kim, D. J. G. In-silico molecular binding prediction for human drug targets using deep neural multi-task learning. 10(11): 906, 2019.
[17] Gasparotto, J., Somensi, N., Bortolin, R. C., Moresco, K. S., Girardi, C. S., Klafke, K., Rabelo, T. K., Morrone, M. D. S., Vizzotto, M., Raseira, M. d. C. B. J. J. o. c. b., and nutrition. Effects of different products of peach (Prunus persica L. Batsch) from a variety developed in southern Brazil on oxidative stress and inflammatory parameters *in vitro* and ex vivo. 55(2): 110-119, 2014.
[18] Gasparotto, J., Somensi, N., Bortolin, R. C., Girardi, C. S., Kunzler, A., Rabelo, T. K., Schnorr, C. E., Moresco, K. S., Bassani, V. L., and Yatsu, F. K. J. J. T. J. o. n. b. Preventive supplementation with fresh and preserved peach attenuates CCl4-induced oxidative stress, inflammation and tissue damage. 25(12): 1282-1295, 2014.
[19] Macarron, R., Banks, M. N., Bojanic, D., Burns, D. J., Cirovic, D. A., Garyantes, T., Green, D. V., Hertzberg, R. P., Janzen, W. P., and Paslay, J. W. Impact of high-throughput screening in biomedical research. *Nature reviews Drug discovery*, 10(3): 188-195, 2011.
[20] Lyu, J., Wang, S., Balius, T. E., Singh, I., Levit, A., Moroz, Y. S., O'Meara, M. J., Che, T., Algaa, E., and Tolmachova, K. Ultra-large library docking for discovering new chemotypes. *Nature*, 566(7743): 224-229, 2019.

[21] Reymond, J.-L. The chemical space project. *Accounts of Chemical Research*, 48(3): 722-730, 2015.
[22] Hall, R. J., Mortenson, P. N., and Murray, C. W. Efficient exploration of chemical space by fragment-based screening. *Progress in biophysics and molecular biology*, 116(2-3): 82-91, 2014.
[23] Browne, R. B., Goswami, N., Borah, P., and Roy, J. D. Computational approaches for evaluation of isobavachin as potential inhibitor against t877a and w741l mutations in prostate cancer. *Journal of Biomolecular Structure and Dynamics*, 41: 2398 - 2418, 2022.
[24] McGann, M. FRED and HYBRID docking performance on standardized datasets. *Journal of Computer-Aided Molecular Design*, 26: 897-906, 2012.
[25] Tietze, S. and Apostolakis, J. GlamDock: Development and Validation of a New Docking Tool on Several Thousand Protein-Ligand Complexes. *Journal of chemical information and modeling*, 47 4: 1657-1672, 2007.
[26] Rarey, M., Kramer, B., Lengauer, T., and Klebe, G. A fast flexible docking method using an incremental construction algorithm. *Journal of molecular biology*, 261 3: 470-489, 1996.
[27] London, N., Miller, R. M., Krishnan, S., Uchida, K., Irwin, J. J., Eidam, O., Gibold, L., Cimermancic, P., Bonnet, R., Shoichet, B. K., and Taunton, J. Covalent Docking of Large Libraries for the Discovery of Chemical Probes. *Nature chemical biology*, 10: 1066 - 1072, 2014.
[28] Kumar, S. and Kumar, S. Molecular Docking: A Structure-Based Approach for Drug Repurposing. *In silico Drug Design*, 2019.
[29] Bartuzi, D., Kaczor, A. A., Targowska-Duda, K. M., and Matosiuk, D. Recent Advances and Applications of Molecular Docking to G Protein-Coupled Receptors. *Molecules : A Journal of Synthetic Chemistry and Natural Product Chemistry*, 22, 2017.
[30] Hsu, K.-C., Chen, Y.-F., Lin, S.-R., and Yang, J.-M. iGEMDOCK: a graphical environment of enhancing GEMDOCK using pharmacological interactions and post-screening analysis. *BMC Bioinformatics*, 12: S33 - S33, 2011.
[31] Thomsen, R. and Christensen, M. H. MolDock: a new technique for high-accuracy molecular docking. *Journal of medicinal chemistry*, 49 11: 3315-3321, 2006.
[32] Tripathi, A. and Misra, K. Inhibition of P-Glycoprotein Mediated Efflux of Paclitaxel by Coumarin Derivatives in Cancer Stem Cells: An *In silico* Approach. *Combinatorial chemistry & high throughput screening*, 19 6: 497-506, 2016.
[33] Lorber, D. M. and Shoichet, B. K. Flexible ligand docking using conformational ensembles. *Protein Science*, 7, 1998.
[34] Tripathi, A. and Misra, K. Designing and Development of Novel Curcumin Analogues/congeners as Inhibitors of Breast Cancer Stem Cells Growth. *Chemical engineering transactions*, 49: 79-84, 2016.
[35] Almi, I., Belaidi, S., Melkemi, N., and Bouzidi, D. J. J. o. B. Chemical reactivity, drug-likeness and structure activity/property relationship studies of 2, 1, 3-benzoxadiazole derivatives as anti-cancer activity. 12(1): 49-57, 2018.
[36] Cheng, F., Li, W., Zhou, Y., Shen, J., Wu, Z., Liu, G., Lee, P. W., and Tang, Y. (ACS Publications, 2012).
[37] Kim, S., Chen, J., Cheng, T., Gindulyte, A., He, J., He, S., Li, Q., Shoemaker, B. A., Thiessen, P. A., and Yu, B. J. N. a. r. PubChem 2019 update: improved access to chemical data. 47(D1): D1102-D1109, 2019.

[38] Seeliger, D. and Groot, B. L. d. Ligand docking and binding site analysis with PyMOL and Autodock/Vina. *Journal of Computer-Aided Molecular Design*, 24: 417 - 422, 2010.
[39] Sali, A. and Blundell, T. L. Comparative protein modelling by satisfaction of spatial restraints. *Journal of molecular biology*, 234 3: 779-815, 1993.
[40] Spoel, D. v. d., Lindahl, E., Hess, B., Groenhof, G., Mark, A. E., and Berendsen, H. J. C. GROMACS: Fast, flexible, and free. *Journal of Computational Chemistry*, 26, 2005.
[41] Lohning, A. E., Levonis, S. M., Williams-Noonan, B. J., and Schweiker, S. S. A Practical Guide to Molecular Docking and Homology Modelling for Medicinal Chemists. *Current topics in medicinal chemistry*, 17 18: 2023-2040, 2017.
[42] Li, D., Zhang, Y., Zhao, R.-N., Fan, S., and Han, J.-G. J. J. o. m. m. Investigation on the mechanism for the binding and drug resistance of wild type and mutations of G86 residue in HIV-1 protease complexed with Darunavir by molecular dynamic simulation and free energy calculation. 20: 1-11, 2014.
[43] Monhemi, H., Housaindokht, M. R., and Nakhaei Pour, A. J. T. J. o. P. C. B. Effects of natural osmolytes on the protein structure in supercritical CO2: molecular level evidence. 119(33): 10406-10416, 2015.